Confinement Size Effect on Crystal Orientation Changes of Poly(ethylene oxide) Blocks in Poly(ethylene oxide)-*b*-polystyrene Diblock Copolymers

Ping Huang,[†] Lei Zhu,[‡] Ya Guo,[†] Qing Ge,[†] Alexander J. Jing,[†] William Y. Chen,[†] Roderic P. Quirk,[†] Stephen Z. D. Cheng,*[,†] Edwin L. Thomas,[§] Bernard Lotz,[⊥] Benjamin S. Hsiao,[#] Carlos A. Avila-Orta,[#] and Igors Sics[#]

Maurice Morton Institute and Department of Polymer Science, The University of Akron, Akron, Ohio 44325-3909; Polymer Program, Institute of Materials Science and Department of Chemical Engineering, The University of Connecticut, Storrs, Connecticut 06269-3136; Department of Materials Science and Engineering, Massachusetts Institute and Technology, Cambridge, Massachusetts 02139; Institute Charles Sadron, 6 Rue Boussingault, Strasbourg 67083, France; and Department of Chemistry, The State University of New York at Stony Brook, Stony Brook, New York 11794-3400

Received October 23, 2003; Revised Manuscript Received March 2, 2004

ABSTRACT: A series of poly(ethylene oxide)-*b*-polystyrene (PEO-*b*-PS) diblock copolymers were designed and synthesized to study the change in crystal orientation of PEO blocks under different confinement sizes. The volume fraction of PEO blocks (f_{PEO}) in these copolymers was kept almost identical (the f_{PEO} values were between 0.45 and 0.48) but with different number-average molecular weights for the PS and PEO blocks ($\bar{M}_n^{PEO}$ and $\bar{M}_n^{PS}$). Therefore, the phase morphology of these copolymers was a lamellar structure with different PEO and PS layer thicknesses (d_{PEO} and d_{PS}) detected by synchrotron small-angle X-ray scattering (SAXS) experiments. Since the melting temperature of these PEO crystals is lower than the glass transition temperature of the PS layers, the PEO block crystals could be melted and recrystallized under one-dimensional (1D) confinement at different crystallization temperatures (T_c). The PEO block crystal orientation changes were monitored using synchrotron wide-angle X-ray diffraction (WAXD) experiments. It was found that the crystalline PEO chain orientation (the *c*-axis in the crystals) underwent a change from being perpendicular (homogeneous) to the layer normal direction ($\hat{n}$) at low T_cs to parallel (homeotropic) at high T_cs in these 1D confined samples with the d_{PEO} ranging from 8.8 to 23.3 nm. However, with the gradual release of this 1D confinement, i.e., increasing the d_{PEO}, a broad T_c region in which the inclined *c*-axis orientation was originally observed in the PEO-*b*-PS with the low $\bar{M}_n^{PEO}$ (8.7K g/mol) and $\bar{M}_n^{PS}$ (9.2K g/mol) became increasingly narrowed by pushing the starting T_c where the tilting initiates toward higher T_c and reducing the ending T_c where the parallel orientation of the *c*-axis with $\hat{n}$ starts. In the PEO-*b*-PS sample with the highest $\bar{M}_n^{PEO}$ (57K g/mol) and $\bar{M}_n^{PS}$ (61.3K g/mol) in this study, this T_c region was narrowed to less than 5 °C, suggesting the confinement size effect on the crystal orientation of the PEO crystals. The homogeneous to homeotropic orientation change of the *c*-axis in the PEO crystals with increasing T_c was explained to be largely governed by the primary nucleation and crystal growth processes of the PEO blocks for developing the maximum crystallinity. A semiquantitative calculation was attempted to illustrate why the homogeneous orientation of the PEO crystals takes place in the 1D confinement based on the SAXS, WAXD, and differential scanning calorimetric results. It was expected that when the d_{PEO} becomes large enough, the homogeneous orientation of the *c*-axis in the PEO crystals would disappear.

Introduction

During the past a few years, investigations of polymer crystallization within confined geometries via crystalline−amorphous diblock copolymers have received substantial attention. Using various ordered phase morphologies such as lamellae, double gyroids, cylinders, and spheres[1] as templates when the systems are below their order−disorder transition temperature (T_{ODT}), the crystalline blocks can be crystallized in a hard-confined environment on a length scale of a few nanometers[2−18] if the glass transition temperature (T_g) of the amorphous blocks is higher than the melting temperature (T_m) of the crystalline blocks. When the T_g is slightly lower than the T_m in a crystalline−amorphous diblock copolymer, the amorphous blocks may construct a soft-confined environment for the crystalline blocks when the crystallization kinetics are fast. Several experimental observations such as the "break-out" crystallization have also been reported. The crystallization behaviors are affected by chain architectures, molecular weights, hardness of the confinements, and confined phase morphologies.[16,18−27]

In one of our recent investigations, a lamellar-forming poly(ethylene oxide)-*b*-polystyrene (PEO-*b*-PS) ($\bar{M}_n^{PEO}$ = 8.7K g/mol and $\bar{M}_n^{PS}$ = 9.2K g/mol) diblock copolymer was studied.[13−15] A large-amplitude oscillating shear was used to generate the macroscopically aligned lamellar phase morphology, and the lamellae normal ($\hat{n}$) was perpendicular to the shear plane. Differential scanning calorimetry (DSC) results showed that the diblock copolymer possessed a glass transition temperature of the PS blocks (T_g^{PS}) of 62 °C and a melting temperature of the PEO blocks (T_m^{PEO}) of ∼51 °C (for a crystallization temperature, T_c, <40 °C). The T_{ODT} was determined to

[†] The University of Akron.
[‡] The University of Connecticut.
[§] Massachusetts Institute and Technology.
[⊥] Institute Charles Sadron.
[#] The State University of New York at Stony Brook.
* To whom correspondence should be addressed. E-mail: scheng@uakron.edu.

10.1021/ma0305378 CCC: $27.50
Published on Web 04/20/2004

Table 1. Molecular Weight and Thermal Properties of a Series of PEO-*b*-PS Samples

sample	$\bar{M}_n^{PS}$ (g/mol)	$\bar{M}_n^{PEO}$ (g/mol)	f_{PEO}	T_{ODT} (°C)	T_g^{PS} (°C)	T_m^{PEO} (°C)
EOS1	9 200	8 700	0.473	160	~62	50
EOS2	26 100	23 100	0.456	190	~79	58
EOS3	61 300	57 000	0.468	>200	~97	64

be 160 °C by temperature-dependent one-dimensional (1D) small-angle X-ray scattering (SAXS) experiments. On the basis of SAXS and transmission electron microscopy observations, the thickness of overall layer spacing ($d_{overall}$), the PS layer (d_{PS}), and the PEO layer (d_{PEO}) was determined to be 18.7, 9.9, and 8.8 nm, respectively. Therefore, the PEO blocks crystallized between two confined glassy PS layers with a space of 8.8 nm.[13]

The T_c dependency of the PEO crystal orientation in the confined lamellae of the diblock copolymer was observed.[13] Four T_c regions have been observed based on the different crystal orientations. (1) For $T_c < -50$ °C (e.g., quickly quenched into liquid nitrogen, N_2, from the melt), the PEO crystals are randomly oriented. (2) Between -50 °C $\le T_c \le -10$ °C, the *c*-axis of the PEO crystals orients perpendicular to $\hat{n}$ (homogeneous). (3) When -5 °C $\le T_c \le 30$ °C, the *c*-axis of the PEO crystals is inclined with respect to $\hat{n}$, where the tilt angle with respect to the shear plane increases with increasing T_c. (4) Finally, for $T_c \ge 35$ °C the *c*-axis of the PEO crystals is parallel to $\hat{n}$ (homeotropic).[13]

In this publication, our focus is to investigate the confined size effect (the d_{PEO}, which is the distance between two neighboring PS layers) on the PEO crystal orientation (the *c*-axis orientation). It is generally expected that with releasing the confined size, i.e., increasing d_{PEO}, the PEO block crystallization should approach to the bulk behavior. In this study, simultaneous 2D SAXS and WAXD experiments show that the crystal orientation, in particular, the T_c region where the *c*-axis of the PEO crystals is inclined with respect to $\hat{n}$ becomes narrowed with increasing d_{PEO}. However, both the homogeneous and homeotropic orientations of the *c*-axis of the PEO crystals with respect to $\hat{n}$ are always observed in a 1D confinement ranging between $d_{PEO} = 8.8$ and 23.3 nm. Furthermore, on the basis of our WAXD, SAXS, and DSC experimental results, we provide a semiquantitative calculation in explaining that the homogeneous *c*-axis orientation in the PEO crystals in the low-T_c region is largely governed by the primary nucleation and crystal growth processes of the PEO blocks for developing the maximum crystallinity.

Experimental Section

Materials and Sample Preparation. A series of PEO-*b*-PS diblock copolymers were synthesized via sequential anionic block copolymerization of styrene and ethylene oxide. Detailed synthesis procedures can be found elsewhere.[15,28] The $\bar{M}_n^{PS}$ precursor was characterized by size exclusion chromatography (SEC) using polystyrene standards. The $\bar{M}_n^{PEO}$ was determined by proton nuclear magnetic resonance (^{1}H NMR), and the polydispersity in the final diblock copolymer was determined by SEC using universal calibration. The detailed molecular characterizations are listed in Table 1. In this table, the volume fraction of the PEO blocks (f_{PEO}) in the melt at 60 °C was calculated on the basis of the densities of amorphous PEO and PS, which are 1.092 and 1.035 g/cm^3, respectively.[15]

To ensure the consistency of the phase behavior, an identical sample preparation procedure was used. The sample was cast from a 5% (w/v) toluene solution, and the solvent was evaporate slowly under a dry nitrogen atmosphere at 50 °C to prevent crystallization of the PEO blocks. Residual solvent was further removed under vacuum at 50 °C. To study the crystal orientation in these copolymers, the samples were subjected to a large-amplitude oscillating shear under a dry argon atmosphere to achieve uniform, parallel alignment of the lamellar phase morphology. The shear frequency was 0.5 Hz, the shear amplitude was 150%, and the shear temperature was higher than both T_g^{PS} and T_m^{PEO} but at least 40 °C below their T_{ODT}. The shear-aligned samples were annealed at 110 °C for 12 h in a vacuum to eliminate residual stresses. The shear direction and resulting lamellar morphology are schematically shown in Figure 1. The $\hat{x}$ direction is the shear direction, and the $\hat{z}$ direction is the shear gradient direction (parallel to $\hat{n}$). The $\hat{x}-\hat{y}$ plane is the shear plane.

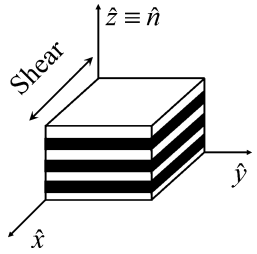

Figure 1. Geometry of the mechanical sheared PEO-*b*-PS copolymers with a lamellar phase morphology.

Equipment and Experiments. Simultaneous 2D SAXS and WAXD experiments were conducted at the synchrotron X-ray beamline X27C at the National Synchrotron Light Source in Brookhaven National Laboratory. The wavelength of the X-ray beam was 0.1366 nm. The zero pixel of the 2D SAXS patterns was calibrated using silver behenate, with the first-order scattering vector q ($q = 4\pi \sin\theta/\lambda$, where λ is the wavelength and 2θ the scattering angle) being 1.076 nm^{-1}. 2D WAXD patterns were calibrated using α-Al_2O_3 with a known crystal diffraction at $2\theta = 28.47°$, and air scattering was subtracted.

To analyze the correlation lengths (apparent crystallite sizes) of the PEO crystals in the 1D confinement, the Scherrer equation was used:

$$D_{hkl} = \frac{K\lambda}{\beta_{hkl} \cos\theta} \tag{1}$$

where D_{hkl} is the mean crystallite size along the [*hkl*] direction and K is the shape factor (the Scherrer constant, a value of 0.94 is used in this case[29]). β_{hkl} is the line breadth, and θ is the half-scattering angle. Usually, β_{hkl} was taken as the half-width at half-maximum (hwhm) of the (*hkl*) diffraction. Assuming that the diffraction peak shape obeyed a Gaussian function, Warren's correction can be used to correct instrument broadening:[29]

$$\frac{\beta_{hkl}}{B_{hkl}} = \sqrt{1 - \frac{b^2}{B_{hkl}^2}} \tag{2}$$

where B_{hkl} is the experimentally observed hwhm of the diffraction peak, and b is the hwhm of a standard specimen diffraction. To ensure a good calibration, the mean crystallite size of the standard specimen should be >60 nm. A quartz line at 60.0° was taken for the standard b. The broadening factor caused by Cu Kα_1 and Kα_2 lines was also taken into account in the calculation.

DSC experiments were carried out on a Perkin-Elmer Pyris Diamond DSC to study melting behaviors of these PEO-*b*-PS samples. The DSC was calibrated with naphthalene, benzoic acid, and indium standards. The fully crystallized samples were heated at a rate of 10 °C/min. The endothermic peak temperature was taken as the melting temperature (T_m). The weight percentage crystallinity (w_c) was calculated using an equilibrium heat of fusion for PEO crystals (8.66 kJ/mol).[30]

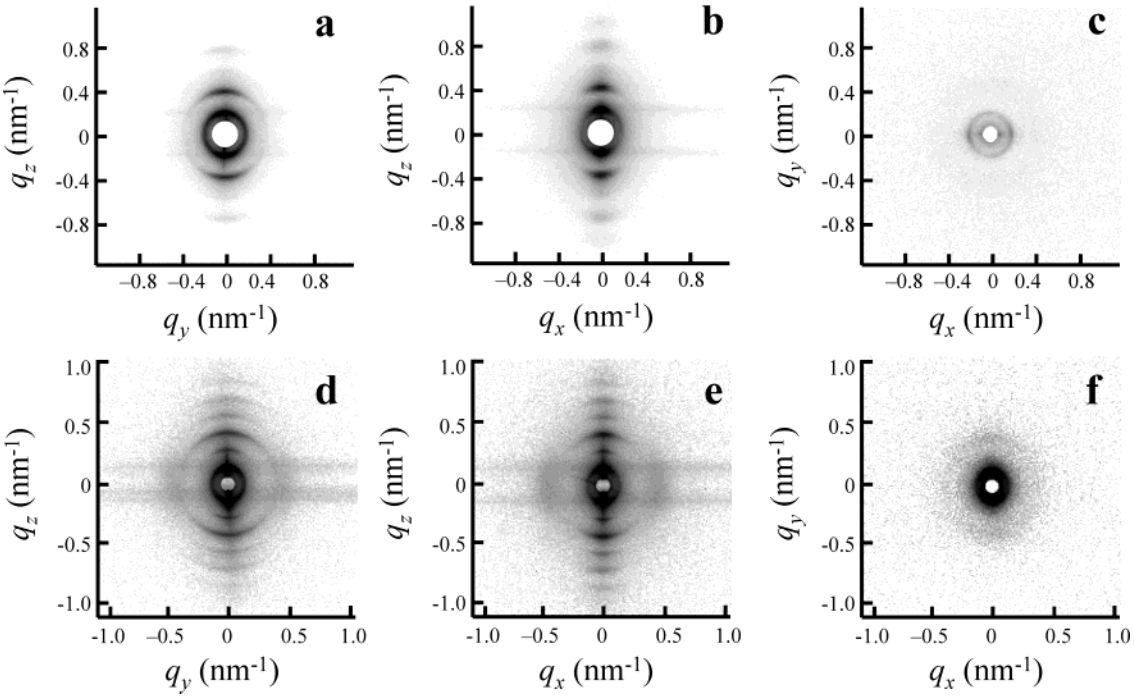

Figure 2. Sets of 2D SAXS patterns of EOS2 at room temperature when the X-ray beam was along (a) the $\hat{x}$, (b) the $\hat{y}$, and (c) the $\hat{z}$ directions and for EOS3 when the X-ray beam was along (d) the $\hat{x}$, (e) the $\hat{y}$, and (f) the $\hat{z}$ directions.

Isothermal crystallization experiments on the shear-aligned samples were conducted using an Instec LN2-P2 hot stage equipped with a liquid N_2 cooling system. The isothermal T_c was controlled to within ±0.2 °C. The samples were preheated to 70 °C for 3 min and then quickly quenched (switched) to the hot stage at a preset T_c for crystallization.

Results and Discussion

Phase Morphology of Different Molecular Weight PEO-*b*-PS Samples. In this series of PEO-*b*-PS diblock copolymers, their f_{PEO} values are in the composition region which exhibits lamellar phase morphology. In Table 1, the first copolymer (EOS1) with $\bar{M}_n^{PEO} = 8.7$K g/mol and $\bar{M}_n^{PS} = 9.2$K g/mol was studied previously, and the data are taken from our previous publications.[13−15] The other two PEO-*b*-PS copolymers with $\bar{M}_n^{PEO} = 23.1$K g/mol and $\bar{M}_n^{PS} = 26.1$K g/mol (EOS2) and $\bar{M}_n^{PEO} = 57.0$K g/mol and $\bar{M}_n^{PS} = 61.3$K g/mol (EOS3) were newly synthesized, and the 2D SAXS and WAXD results are first time reported here. Table 1 also lists the transition temperatures for this series of block copolymers. For all these three samples, the hard confinement criteria, $T_{ODT} > T_g^{PS} > T_m^{PEO}$, are held, and therefore, the crystallization of PEO blocks take place between two neighboring glassy PS layers.[11]

To verify the phase morphology, Figure 2a−f exhibits a series of 2D SAXS patterns that were taken at room temperature when the X-ray beam was directed along the $\hat{x}$, $\hat{y}$, and $\hat{z}$ directions for EOS2 and EOS3. Similar with the 2D SAXS patterns for EOS1 in our previous work (Figure 3 in ref 13), the SAXS patterns for EOS2 and EOS3 along both the $\hat{x}$ and $\hat{y}$ directions show the multiple ordered diffractions with a ratio of 1:2:3 ..., indicating that these three samples possess the lamellar phase morphology. Despite different T_c values in the crystallization, the 2D SAXS patterns were always identical, revealing that the lamellar morphology was retained after the crystallization process. This provides experimental evidence that the PEO blocks crystallized in the 1D hard confinement.

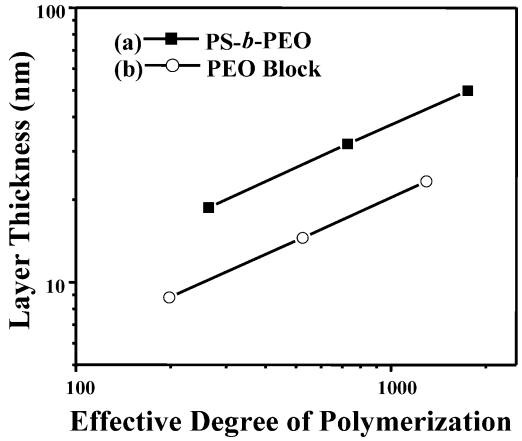

Figure 3. Relationships between (a) logarithmic $d_{overall}$ and logarithmic N_e of the diblock copolymer and (b) logarithmic d_{PEO} and logarithmic N_{PEO} in this series of PEO-*b*-PS diblock copolymers.

Table 2. Degrees of Polymerization and Layer Thicknesses of a Series of PEO-*b*-PS Samples

sample	N_{PS}[a]	N_{PEO}[a]	N_e[a]	$d_{overall}$ (nm)	d_{PEO} (nm)	d_{PS} (nm)
EOS1	88	198	264	18.7	8.8	9.9
EOS2	251	525	729	31.9	14.5	17.4
EOS3	589	1295	1750	49.8	23.3	26.5

[a] N_{PS} and N_{PEO} are number-average degrees of polymerizations of the PS and PEO blocks. N_e is the effective degree of polymerization, which has been corrected for the asymmetry in the segment sizes of the PEO and PS and blocks. $N_e = (v_{EO}/v_0)N_{PEO} + (v_{St}/v_0)N_{PS}$, where $v_0 = (v_{EO}v_{St})^{1/2}$, and the v_{EO} and v_{St} are the volumes of PEO and PS monomers, respectively.

From the 2D SAXS patterns in Figure 2, the $d_{overall}$ values were obtained and are listed in Table 2. It is evident that the $d_{overall}$ increases with the molecular weight of the PEO-*b*-PS copolymers. Table 2 also includes the d_{PEO} values, which are calculated on the basis of the f_{PEO} values. They are also increased with the molecular weights of the PEO and PS blocks.

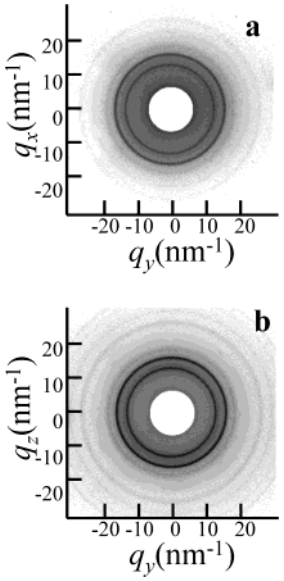

Figure 4. Set of 2D WAXD patterns of EOS2 crystallized after being quenched into liquid nitrogen: (a) the X-ray beam was along the $\hat{z}$ direction; (b) the X-ray beam was along the $\hat{x}$ direction.

Changes of $d_{overall}$ with degree of polymerization, N, could be used to interpret the segregation regimes.[31] On the basis of the mean-field prediction, it was reported that $d_{overall}$ is proportional to N^{α}, and the α value decreases continuously from 0.95 at the critical point between the weak and the strong segregation regimes to 0.67 in the strong segregation regime.[32] In our samples, the effective degree of polymerization, N_e, should be used in this relationship between the $d_{overall}$ and the N_e due to the asymmetry in the segment sizes of the PEO and PS blocks. The detailed calculation of the N_e values can be found in one of our previous publications,[15] and the values are also listed in Table 2.

Figure 3 shows two relationships, one of which is the logarithmic $d_{overall}$ with respect to the logarithmic N_e, and the other is the logarithmic d_{PEO} with respect to the logarithmic N_{PEO} for this series of PEO-*b*-PS diblock copolymers. It is found that the α value is 0.52 for both these two relationships. Usually, a small α value suggests the strong segregation at room temperature of the PEO-*b*-PS block copolymer samples. Surprisingly, however, this α value is lower than the theoretical value even in the strong segregation regime.[32] One of the possible reasons may be that our samples are not precisely symmetric block copolymers (the volume fraction is not equal to 0.5). Further investigation is necessary to fully explain this observation.

Crystal Orientation Changes at Different T_c under Varying d_{PEO} Values. Using 2D WAXD patterns, the PEO crystal orientation changes with respect to T_c could be observed. We report the 2D WAXD patterns of EOS2 as a representative. In addition, since samples with a lamellar phase morphology give the identical 2D WAXD patterns when the X-ray beam was directed along the $\hat{x}$ and $\hat{y}$ directions, we only show the patterns with the X-ray beam directed along the $\hat{x}$ direction.

When the samples were quenched to liquid N_2, Figure 4a,b shows the 2D WAXD patterns when the X-ray beam was directed along the $\hat{z}$ and $\hat{x}$ directions. Both the patterns show isotropic (ring) diffractions that indicate a random crystal orientation within the confined lamellae. During the liquid N_2 quenching process, a large number of homogeneous nucleation sites are created. It is speculated that the primary nucleation density is so high that little crystal growth is needed to complete crystallization. The crystals generated are too small in size to feel the PS layer confinement. Both these two PEO-*b*-PS copolymers exhibit the random crystal orientation when they were quenched into liquid N_2.

When the mechanically shear-aligned EOS2 is quickly quenched from 70 °C to T_c values between −40 and 0 °C, their 2D WAXD patterns having the X-ray beam directed along the $\hat{z}$ and $\hat{x}$ directions are shown in Figure 5a−i. Since the 2D WAXD patterns in Figure 5a,d,g are isotropic when the X-ray beam was directed along the $\hat{z}$ direction, the *c*-axis of PEO crystals is macroscopically isotropic with respect to $\hat{n}$. However, the 2D WAXD patterns in Figure 5b,e,h when the X-ray beam was directed along the $\hat{x}$ direction give rise to the oriented (120) reflections (*d*-spacing of 0.463 nm) with the major intensity along the $\hat{z}$ direction and the minor intensity in the $\hat{x}-\hat{y}$ plane. This can be clearly observed in the azimuthal scans, as shown in Figure 5c,f,i. Other diffractions having smaller *d*-spacings are also oriented correspondingly and analyzed following the procedure described in ref 13. These diffraction patterns can be qualitatively explained using a [120] uniaxial pattern with the [120] $\equiv \hat{n}$.[13] One can thus conclude that the *c*-axis of the PEO crystals is approximately perpendicular to $\hat{n}$ and randomly distributed in the $\hat{x}-\hat{y}$ plane. Note that in this case the *b*-axis of the PEO crystals tilts about 45° from $\hat{n}$. Moreover, the T_c region in which the *c*-axis of the PEO crystals is perpendicular to $\hat{n}$ changes with $\bar{M}_n^{PEO}$. For the lowest molecular weight sample in this series (EOS1), the T_c at which the PEO crystals had the homogeneous orientation ended at −10 °C.[13] This temperature increases to 0 °C for the intermediate molecular weight sample of EOS2. For the highest molecular weight sample of EOS3, it is further increased to 10 °C.

Figure 6a−f shows the 2D WAXD patterns of EOS2 when the X-ray beam was directed along the $\hat{z}$ and $\hat{x}$ directions after the shear-aligned sample is crystallized at a T_c between 5 and 15 °C. The 2D WAXD patterns when the X-ray beam was directed along the $\hat{z}$ direction are again isotropic (Figure 6a,c,e), indicating the random *c*-axis orientation in the PEO crystals with respect to $\hat{n}$. In Figure 6b,d,f, 2D WAXD patterns when the X-ray beam was directed along the $\hat{x}$ direction show that the (120) diffractions are located in both the quadrants and on the $\hat{x}-\hat{y}$ plane, while those on the $\hat{z}$ direction vanish. With increasing T_c, the diffractions in the quadrants gradually move toward the diffraction pair on the $\hat{x}-\hat{y}$ plane. Following our previous analysis,[13] these diffraction patterns reveal an inclined crystal orientation with respect to $\hat{n}$, and the tilt angle of the crystal *c*-axis away from the $\hat{x}-\hat{y}$ plane gradually increases with increasing T_c, while being randomly distributed around $\hat{n}$. The T_c region where the *c*-axis of the PEO crystals is inclined with respect to $\hat{n}$ decreases with increasing $\bar{M}_n^{PEO}$.

After EOS2 sample was isothermally crystallized at T_c values which are higher than 15 °C, 2D WAXD patterns obtained when the X-ray beam was directed along the $\hat{z}$ and $\hat{x}$ directions are shown in Figure 7a−f. The 2D WAXD patterns when the X-ray beam was

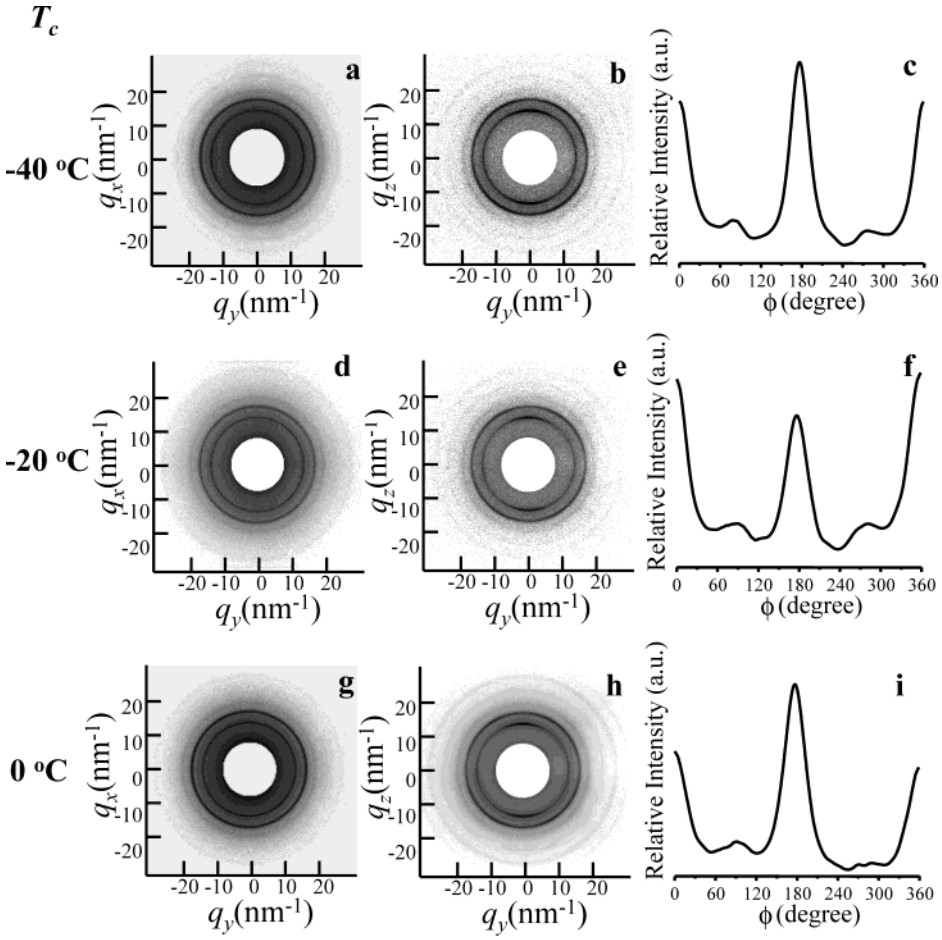

Figure 5. Set of 2D WAXD patterns of EOS2 in the T_c region with the homogeneous *c*-axis orientation of the PEO crystals: (a) $T_c = -40$ °C, the X-ray beam was along the $\hat{z}$ direction; (b) $T_c = -40$ °C, the X-ray beam was along the $\hat{x}$ direction; (c) an azimuthal scanning of the (120) diffractions of (b); (d) $T_c = -20$ °C, the X-ray beam was along the $\hat{z}$ direction; (e) $T_c = -20$ °C, the X-ray beam was along the $\hat{x}$ direction; (f) an azimuthal scanning of the (120) diffractions of (e); (g) $T_c = 0$ °C, the X-ray beam was along the $\hat{z}$ direction; (h) $T_c = 0$ °C, the X-ray beam was along the $\hat{x}$ direction; (i) an azimuthal scanning of the (120) diffraction of (h).

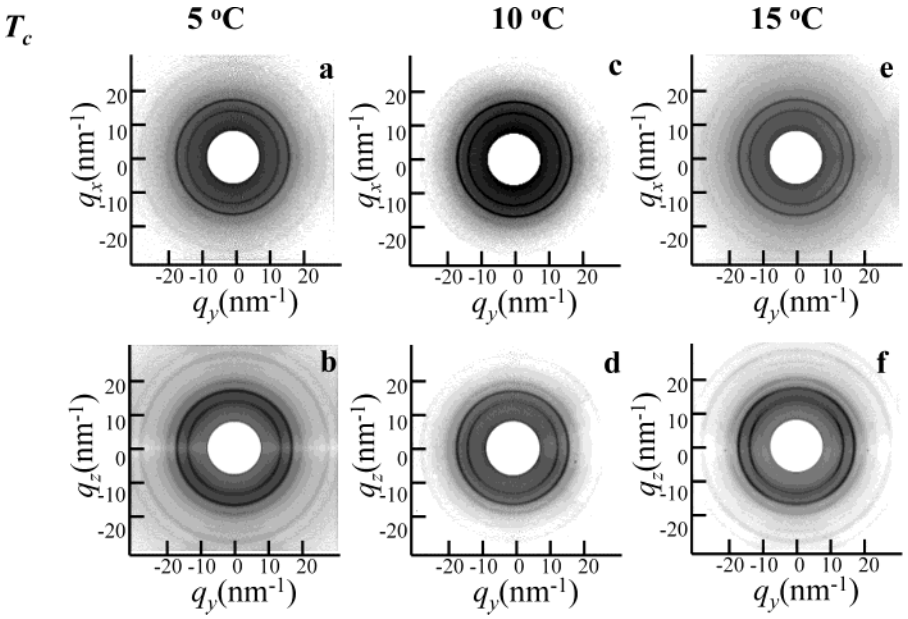

Figure 6. Set of 2D WAXD patterns of EOS2 crystallized in the T_c region with the inclined *c*-axis orientation of the PEO crystals. (a) $T_c = 5$ °C, the X-ray beam was along the $\hat{z}$ direction; (b) $T_c = 5$ °C, the X-ray beam was along the $\hat{x}$ direction; (c) $T_c = 10$ °C, the X-ray beam was along the $\hat{z}$ direction; (d) $T_c = 10$ °C, the X-ray beam was along the $\hat{x}$ direction; (e) $T_c = 15$ °C, the X-ray beam was along the $\hat{z}$ direction; (f) $T_c = 15$ °C, the X-ray beam was along the $\hat{x}$ direction.

directed along the $\hat{x}$ direction in Figure 7b,d,f show that the (120) reflection pairs are exclusively in the $\hat{x}-\hat{y}$ plane. This indicates that the *c*-axis of PEO crystals is oriented parallel to $\hat{n}$. This pattern is identical to the

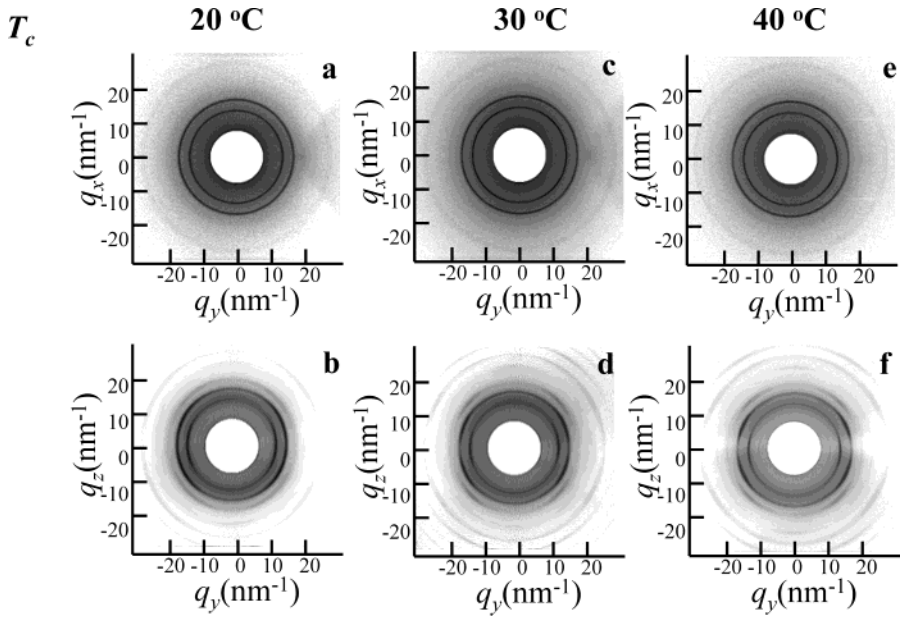

Figure 7. Set of 2D WAXD patterns of EOS2 crystallized in the T_c region with homeotropic *c*-axis orientation of the PEO crystals: (a) $T_c = 20$ °C, the X-ray beam was along the $\hat{z}$ direction; (b) $T_c = 20$ °C, the X-ray beam was along the $\hat{x}$ direction; (c) $T_c = 30$ °C, the X-ray beam was along the $\hat{z}$ direction; (d) $T_c = 30$ °C, the X-ray beam was along the $\hat{x}$ direction; (e) $T_c = 40$ °C, the X-ray beam was along the $\hat{z}$ direction; (f) $T_c = 40$ °C, the X-ray beam was along the $\hat{x}$ direction.

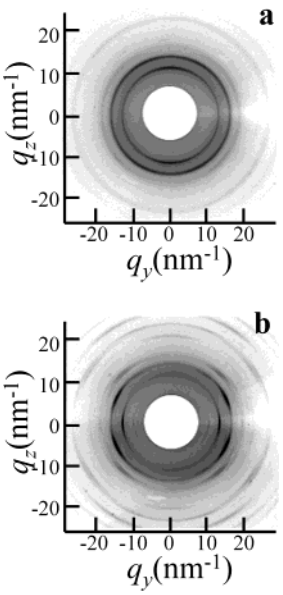

Figure 8. Set of 2D WAXD patterns of EOS3 crystallized at (a) $T_c = -20$ °C in the homogeneous *c*-axis orientation of the PEO crystals and at (b) $T_c = 30$ °C in the homeotropic *c*-axis orientation of the PEO crystals. The X-ray beam was along the $\hat{x}$ direction.

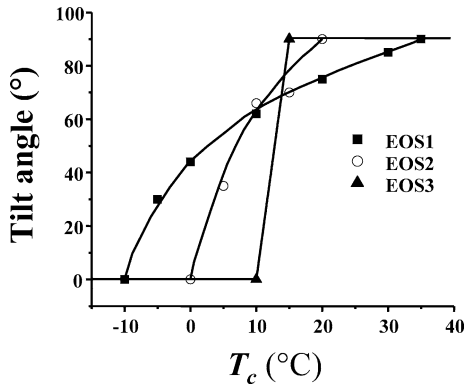

Figure 9. Relationships between the inclined angles with respect to T_cs for different PEO-*b*-PS copolymers.

WAXD fiber pattern.[33] The isotropic 2D WAXD patterns obtained when the X-ray beam was directed along the $\hat{z}$ direction in Figure 7a,c,e again demonstrate that the crystal orientation is randomly distributed with respect to $\hat{n}$. Parts a and b of Figure 8, which were taken when the X-ray was aligned along the $\hat{x}$ direction, show two different *c*-axis orientations of the PEO blocks in EOS3 crystallized at $T_c = -20$ and 30 °C. Figure 8a exhibits the homogeneous *c*-axis orientation, while Figure 8b represents the homeotropic *c*-axis orientation in the PEO crystals. It is interesting that the starting T_c, where the *c*-axis is found to be parallel to $\hat{n}$, decreases with increasing the $\bar{M}_n^{PEO}$. For EOS1 with a $\bar{M}_n^{PEO} =$ 8.7K g/mol, the T_c, where the PEO crystals homeotropic orientation starts, is at 35 °C,[13] and this temperature decreases to 20 °C for EOS2 with a $\bar{M}_n^{PEO} = 23.1$K g/mol. For EOS3 with a $\bar{M}_n^{PEO} = 57.0$K g/mol, this T_c further decreases to 15 °C.

Figure 9 shows the inclined *c*-axis angle changes with respect to T_c for this series of PS-*b*-PEO diblock copolymers. When the samples were quenched to liquid N_2 from the PEO melt at 70 °C, the PEO crystals are randomly oriented in between two PS confined layers. With increasing T_c, a temperature region appeared where the *c*-axis of the PEO crystals is perpendicular to $\hat{n}$, yet randomly oriented in the $\hat{x}-\hat{y}$ plane. Further increasing T_c, a temperature region is reached where the *c*-axis is inclined with respect to $\hat{n}$. Continuously increasing the T_c leads to a gradual change of the *c*-axis in the PEO crystals toward $\hat{n}$. Finally, in the highest T_c region, the *c*-axis of the PEO crystals is parallel to $\hat{n}$. Furthermore, with increasing the $\bar{M}_n^{PEO}$, the T_c region where the *c*-axis of the PEO crystals is perpendicular to $\hat{n}$ expands toward higher T_c values, while the T_c region where the *c*-axis of the PEO crystals is parallel to $\hat{n}$ expands toward lower T_c values. Consequently, this leads to a decrease in range of the T_c region where the *c*-axis of the PEO crystals is inclined with respect to $\hat{n}$.

Table 3. PEO Crystallinity and Crystals Size Estimations in the T_c Regions Where the *c*-Axis of PEO Crystals Is in the Homogeneous Orientation for EOS2 and EOS3 Samples

sample	T_c (°C)	w_c[a]	v_c[b]	$D_{120,\perp}$[c] (nm)	$D_{120,\parallel}$[c] (nm)	L_{PEO}[d] (nm)	n_{PEO}[e] (nm^{-3})	V_{PEO}[f] (nm^3)	l_{PEO}[g] (nm)
EOS2	−40	0.46	0.44	9.7	12.2	11.0	0.000 57	772	6.5
	−30	0.46	0.44	10.4	12.3	11.4	0.000 53	830	6.5
	−20	0.46	0.44	10.8	12.8	11.6	0.000 51	863	6.3
	−10	0.43	0.41	10.9	13.0	12.1	0.000 47	872	6.2
	0	0.42	0.40	10.6	12.6	13.1	0.000 40	1000	7.5
EOS3	−40	0.51	0.49	11.5	14.1	12.6	0.000 27	1815	11.2
	−30	0.51	0.49	12.1	15.0	13.0	0.000 25	1960	10.8
	−20	0.50	0.48	12.2	15.3	13.5	0.000 24	2000	10.7
	−10	0.49	0.47	12.3	16.4	14.1	0.000 22	2136	10.6
	0	0.48	0.46	11.8	15.4	14.3	0.000 21	2190	12.1
	5	0.48	0.46	11.4	15.0	14.5	0.000 20	2300	13.5
	10	0.48	0.46	11.7	15.1	15.2	0.000 19	2476	14.0

[a] PEO weight percentage crystallinities, obtained in DSC experiments. [b] PEO volume percentage crystallinities, $v_c = \rho_a w_c/[\rho_a w_c + \rho_c(1 - w_c)]$, where ρ_c and ρ_a are the density of crystalline and amorphous PEO, respectively. [c] The lateral crystallite sizes of PEO crystal calculated based on the Sherrer equation. [d] The average distances of the PEO crystals obtained in the azimuthally integrated 2D SAXS patterns. [e] The primary nucleation densities of the PEO crystals, $n_{PEO} = 1/(L_{PEO}^2 d_{PEO})$. [f] The average volumes per PEO crystals, $V_{PEO} = v_c/n_{PEO}$. [g] The calculated thicknesses of the PEO crystals, $l_{PEO} = V_{PEO}/(D_{120,l}D_{120,s})$.

Confined Size Effect on Crystal Orientation Changes. As shown in Figure 9, two *c*-axis orientations in the PEO crystals exist for this series of diblock copolymers: the homogeneous and the homeotropic orientations with respect to $\hat{n}$. The question is, why do we observe both of these orientations in the PEO crystals in the low- and high-T_c regions? In the case of EOS1, it was speculated that the homogeneously oriented PEO crystals grown in the low-T_c region may be influenced by two factors. The first is that the PEO crystal thickness along the *c*-axis (l_{PEO}) may be equal to or larger than the d_{PEO} for EOS1 (8.8 nm). The second factor is that the primary nucleation density is high, and thus, only the nucleation takes place, and the crystal growth is limited in this T_c region. To achieve the maximum crystallinity, the PEO crystals have to take the homogeneous *c*-axis orientation.[13] However, in the case of EOS3, the d_{PEO} is 23.3 nm, and it must be larger than the values of l_{PEO}. Therefore, it is necessary to reexamine the factors that force the PEO blocks to adopt the homogeneous *c*-axis orientation in the 1D confinement.

To provide a semiquantitative calculation, we assume that within two neighboring PS glassy layers the PEO blocks form individual crystals (no multiple crystal stacking; see below). They are randomly distributed in the $\hat{x}-\hat{y}$ plane, while their *c*-axis is perpendicular to $\hat{n}$ in the low-T_c region. The PEO crystals grow along the two pairs of the [120] directions that are perpendicular to each other. One pair of the [120] growth direction is parallel to $\hat{n}$, and another pair of the [120] direction is perpendicular to $\hat{n}$. The former pair of (120) planes cannot grow far due to the confinement of the neighboring PS glassy layers (d_{PEO}).[13−15]

In this assumed model, one of the most important parameters is the l_{PEO}. Because of a strong scattering generated by the PS blocks in the low-frequency region of Raman spectroscopy, longitudinal acoustical mode of low-frequency Raman spectroscopy to determine the l_{PEO} for PEO crystals[27,34−36] cannot be utilized. Hence, an indirect calculation is designed to find the l_{PEO}. If we know the average distance between the PEO crystals in the $\hat{x}-\hat{y}$ plane, L_{PEO}, we can calculate the average primary nucleation density of the PEO crystals (n_{PEO}) as a first approximation:

$$n_{PEO} = 1/(L_{PEO}^2 d_{PEO}) \quad (3)$$

On the other hand, the average volume per PEO crystal, V_{PEO}, can be calculated as

$$V_{PEO} = v_c/n_{PEO} \quad (4)$$

where the v_c is the volume percentage crystallinity of PEO crystals. It can be calculated by

$$v_c = \frac{\rho_a w_c}{\rho_a w_c + \rho_c(1 - w_c)} \quad (5)$$

where the w_c is the weight percentage crystallinity of the PEO crystals. The values of ρ_c and ρ_a are the densities of crystalline and amorphous PEO, respectively. At room temperature, $\rho_c = 1.239$ g/cm^3 and $\rho_a = 1.124$ g/cm^3.[37]

The value of l_{PEO} can thus be calculated following the equation of

$$l_{PEO} = V_{PEO}/(D_{120,\parallel}D_{120,\perp}) \quad (6)$$

where the $D_{120,\parallel}$ and $D_{120,\perp}$ are dimensions of the PEO crystals along both the [120] directions which are parallel and perpendicular to $\hat{n}$. Note that in this simple model we only obtain the average structural parameters and do not take specific considerations of the effect of interfaces between the PEO and PS layers on these parameters.

We therefore need experimental results to calculate these parameters. First, the L_{PEO} values are necessary to know. Careful examinations of our 2D SAXS patterns of EOS2 and EOS3 when the X-ray beam was directed along the $\hat{z}$ direction lead to an observation that the scattering rings resulted from the PEO crystals in the $\hat{x}-\hat{y}$ plane in the T_c regions where the *c*-axis is in the homogeneous orientation. Parts a and b of Figure 10 show 1D SAXS patterns at different T_c values for EOS2 and EOS3 when X-ray beam is along the $\hat{z}$ direction, respectively. Both figures were generated by azimuthal integrations of the 2D SAXS patterns. It is evident that these are broad scattering halos. The central positions of these scattering halos are taken as the L_{PEO} values for EOS2 and EOS3, as they are listed in Table 3. These scattering halos can also be observed in the 2D SAXS patterns when the X-ray beam was along the $\hat{x}$ direction, as shown in Figure 11 for EOS2 and EOS3 at $T_c = -30$ °C as two examples. Both patterns show weak and broad

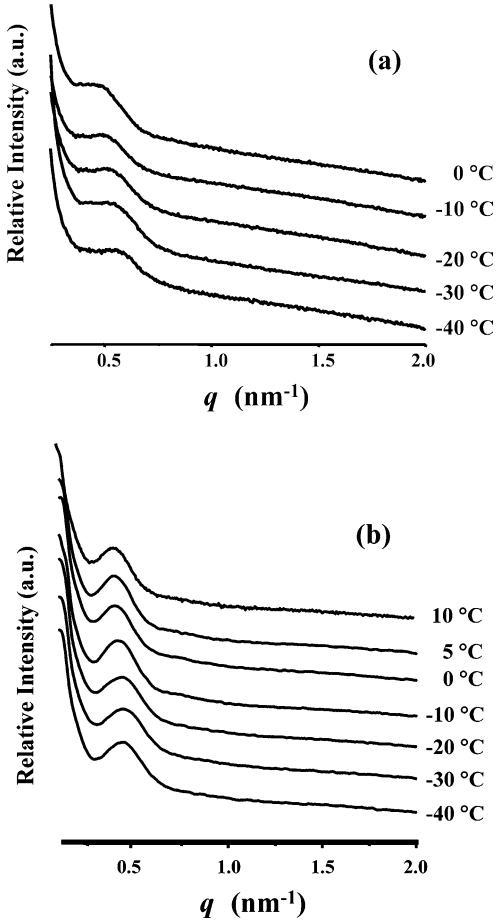

Figure 10. Set of 1D SAXS patterns with the homogeneous *c*-axis orientation of the PEO crystals (a) for EOS2 and (b) for EOS3.

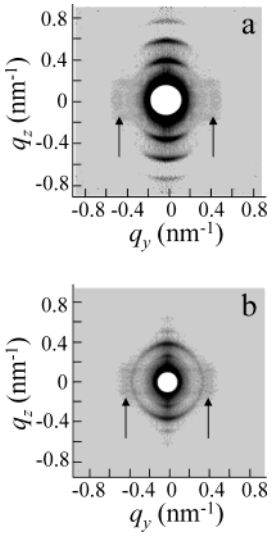

Figure 11. Two 2D SAXS patterns of EOS2 (a) and EOS3 (b) when X-ray beam was along the $\hat{x}$ direction with the homogeneous *c*-axis orientation of the PEO crystals at $T_c = -30$ °C. The scattering halos located along the $\hat{y}$ directions as pointed out by the arrows in these patterns.

scattering halos on the $\hat{y}$ (horizontal)-axis, as pointed out by the arrows in the figures.

It should also be noted that after the *c*-axis of PEO crystals is inclined or parallel to $\hat{n}$, the scattering halos in the SAXS patterns become very diffused, and it is difficult to have a quantitative study. This may be due to the fact that the *c*-axis of the PEO crystals is in the

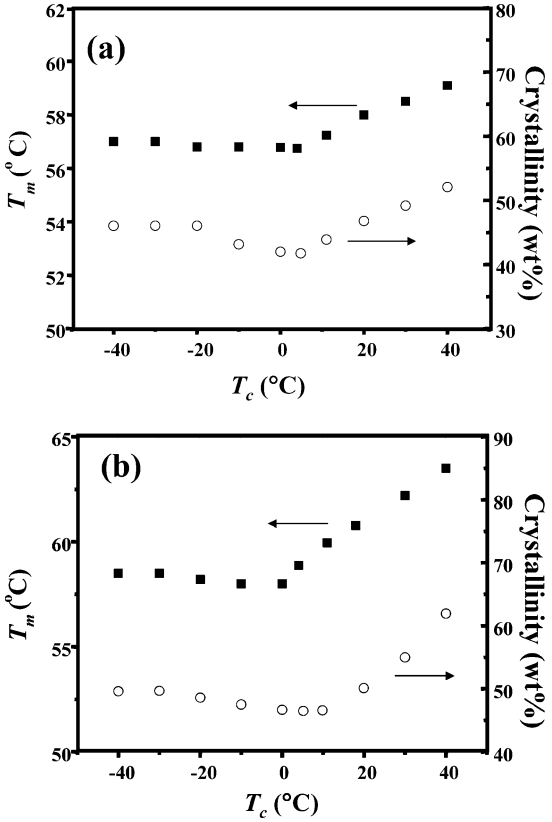

Figure 12. Changes of the crystallinities and melting temperatures with respect to T_c: (a) for EOS2 and (b) for EOS3.

inclined or the parallel orientations with respect to $\hat{n}$ smears the electron density period. In the case of EOS1, the 2D SAXS patterns when the X-ray beam was directed along the $\hat{z}$ direction exhibit weak, residual scattering of the $d_{overall}$, and this scattering is overlapped with the scattering ring resulting from the PEO crystals in the $\hat{x}-\hat{y}$ plane in the T_c region. The information on the L_{PEO} and l_{PEO} of EOS1 cannot be precisely discerned from the overlapped scatterings, and thus, they are not going to be discussed.

Next step is to know the v_c of the PEO crystals, which can be calculated from the w_c of PEO crystals based on eq 5. The w_c values for EOS2 and EOS3 are obtained from DSC measurements. Parts a and b of Figure 12 show the T_m and w_c changes with respect to T_c for EOS2 and EOS3, respectively. For EOS2, the T_m keeps almost constant of ~57 °C when $T_c \leq 0$ °C, and the w_c values are slightly changed between 0.42 and 0.46. When $T_c > 0$ °C, both of them increase with increasing T_c. At $T_c = 40$ °C, the T_m reaches 59 °C, and the w_c is slightly higher than 0.50. The T_m and w_c for EOS3 also exhibit similar T_c dependences, but with higher T_m and w_c values compared with those of EOS2 when they are crystallized under the same conditions. These higher T_m and w_c values of EOS3 may result from the higher molecular weight and large crystal sizes of EOS3.

The last set of parameters we need to know is the $D_{120,\parallel}$ and $D_{120,\perp}$. We can estimate these values on the basis of the correlation lengths of the [120] direction parallel and perpendicular to $\hat{n}$ calculated using the Sherrer equation.[14] Parts a and b of Figure 13a and 13b show the correlation lengths of the [120] direction changes with respect to T_c for EOS2 and EOS3, respectively. As shown in Figure 13a in the region of -40 °C $\leq T_c \leq 0$ °C, the $D_{120,\parallel}$ values of the PEO crystals in

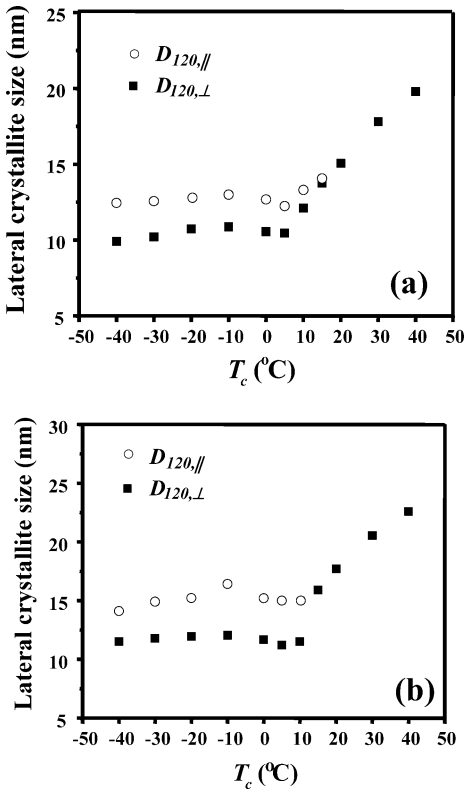

Figure 13. Correlation length (apparent crystallite size) analyses for the (120) diffractions at different T_c values in the 2D WAXD patterns when X-ray beam is along the $\hat{x}$ direction: (a) for EOS2 and (b) for EOS3.

EOS2 are slightly thicker than those of $D_{120,\perp}$, indicating that the crystal growth in the $\hat{x}-\hat{y}$ plane is more constrained than that along $\hat{n}$. Note that the confinement on the PEO crystal growth along $\hat{n}$ comes from the PS glassy layer. In the $\hat{x}-\hat{y}$ plane, the confinement is caused by an impingement of neighboring crystals, which is determined by the n_{PEO}. In this T_c region, both the $D_{120,||}$ and $D_{120,\perp}$ values gradually and slightly increases with increasing T_c, up to −10 °C, slightly different from the observations in EOS1 where the $D_{120,||}$ values are constant and the $D_{120,\perp}$ values slightly increase in this T_c region.[14] Note that the upper limits of the $D_{120,||}$ for EOS2 is $d_{PEO} = 14.5$ nm. The calculated $D_{120,||}$ values in EOS2 ranged between 12 and 13 nm along $\hat{n}$ should reflect actual crystal sizes. The calculated $D_{120,\perp}$ of EOS2 is between 9.7 and 10.9 nm. Compared with their L_{PEO} values of 11−13 nm as listed in Table 3, they should also represent actual crystal sizes. A similar trend can also be found in the case of EOS3, as shown in Figure 13b. However, for EOS3, the $D_{120,||}$ values do not reach the d_{PEO} value (23.3 nm), but only 60%−70% of this value, while the $D_{120,\perp}$ values are thinner than those of L_{PEO} (Table 3).

In Figure 13a,b, a maximum can be found for both the $D_{120,||}$ and $D_{120,\perp}$ values at around $T_c = -10$ °C. These phenomena may be associated with a change of nucleation mechanism from homogeneous to heterogeneous nucleation.[14] As soon as the T_c enters the region where the *c*-axis of the PEO crystals starts to incline, the $D_{120,\perp}$ values for both cases continuously increase, and the $D_{120,||}$ values also increase, and finally merge with the $D_{120,\perp}$ values. Both of the values gradually lose their representatives of the actual crystal sizes. These observations are identical to those observations in EOS1.[14]

By knowing the L_{PEO} values, the n_{PEO} values can be calculated based on eq 3 and listed in Table 3 for EOS2 and EOS3 within the T_c region where the homogeneous *c*-axis orientation of the PEO crystals is observed. The n_{PEO} decreases slightly with increasing T_c for both EOS2 and EOS3. Moreover, the n_{PEO} values for EOS2 are higher than those of EOS3. On the basis of the w_c values obtained from the DSC results, we can calculate the v_c values using eq 5 and, thus, the V_{PEO} values based on eq 4. Since we know the $D_{120,||}$ and $D_{120,\perp}$ values for EOS2 and EOS3, their l_{PEO} values are obtained using eq 6. These experimental and calculated results are also listed in Table 3. Since both of the $D_{120,||}$ and $D_{120,\perp}$ values are considered to be actual crystal sizes in this T_c region, the PEO crystals of EOS2 and EOS3 in this T_c region are on the nanometer scale in all three dimensions.

In both of EOS2 and EOS3 cases, most of their d_{PEO} values are more than twice of the l_{PEO} in this low-T_c region. The question is, why do the PEO crystals not adopt the homeotropic *c*-axis orientation (parallel to $\hat{n}$)? Note that the overall PEO crystal thickness along the *c*-axis is thicker than l_{PEO} (due to additional two crystal interfaces). If the PEO crystals would adopt the homeotropic *c*-axis orientation, only one layer of polycrystalline PEO crystals can be hosted by each d_{PEO}. This could lead to a lower w_c value compared with the experimentally observed w_c values. On the other hand, if the d_{PEO} would host more than one PEO crystals having the homeotropic *c*-axis orientation, the stacked crystals must be in different sizes, and thus, they would possess different metastability.[39,40] Therefore, in DSC experiments, we had to observe more than one T_m endotherms. However, only a single sharp melting endotherm in the DSC thermal diagrams was observed. Therefore, we conclude that in order to achieve higher w_c values, the PEO crystals have to adopt the homogeneous *c*-axis orientation. Only when the d_{PEO} is sufficiently thick to approach bulklike behavior (say, the d_{PEO} reaches submicrometers) can the *c*-axis homogeneous orientation of the PEO crystals disappear. It is known that PEO thin film samples with thicknesses ranging from tens to hundreds of nanometers contain PEO crystals where the *c*-axis adopts the homeotropic orientation. In those cases, however, the PEO molecules do not have hard confinement at the air−crystal interface.[41,42]

Furthermore, there is the T_c region where the *c*-axis is inclined in between two T_c regions having the homogeneous and homeotropic orientations. By increasing the $\bar{M}_n^{PEO}$ and keeping the volume fraction almost constant, the width of this T_c region decreases. In the case of EOS1, the temperature region where the *c*-axis is inclined is 45 °C (between −10 and 35 °C). For EOS2, this temperature range decreases to 20 °C (between 0 and 20 °C). In the case of EOS3, this range is less than 5 °C (between 10 and 15 °C). It is evident that the d_{PEO} values which range between 8.8 and 23.3 nm are critically important in affecting the T_c region where the *c*-axis is inclined with respect to $\hat{n}$. This leads to an extrapolation that above a d_{PEO} of ∼25 nm the inclined *c*-axis orientation may disappear. Note that the crystal sizes continuously increase with increasing T_c in this inclined *c*-axis T_c region, indicated by the T_m and the $D_{120,||}$ and $D_{120,\perp}$ values increase, as shown in Figures 12 and 13. We speculate that this inclined orientation may be caused by a compromise between the n_{PEO} (which is not high enough to limit the neighboring PEO

crystal growth) and the crystal growth (which is not too fast for the pair of [120] directions parallel to $\hat{n}$) within the 1D confinement. A free energy expression for the crystal formation in 1D confinement must not only include the traditional bulk and surface free energies but also include a term for the energy resulted from the 1D confinement. Therefore, the PEO crystals with a specific inclined angle of the *c*-axis at each T_c must possess a local free energy minimum due to the effect of their neighboring PS glassy layers. It is predicted that the inclined *c*-axis orientation in these diblock copolymers is controlled by kinetics in the 1D-confined lamellae. Quantitative analyses of these kinetic processes require the experimental observation of the nucleation and growth data in the PEO-*b*-PS diblock copolymers.

Conclusion

In summary, we have investigated the effect of 1D confinement of various sizes (d_{PEO}) on crystal orientation changes in the lamellar phase morphology using a series of PEO-*b*-PS samples with different $\bar{M}_n^{PEO}$ and $\bar{M}_n^{PS}$. It has been found that the most dominant effect of d_{PEO} between 8.8 and 23.3 nm is on the T_c regions where the *c*-axis of PEO crystal orientation is inclined. With increasing the d_{PEO} values, this T_c region quickly narrows, and finally, it should disappear when the d_{PEO} reaches ~25 nm. In these PEO-*b*-PS samples, both the homogeneous *c*-axis orientation of the PEO crystals in the low-T_c region and the homeotropic *c*-axis orientation in the high-T_c region are observed. The homogeneous *c*-axis orientation may diminish when the d_{PEO} arrives in thicknesses of above submicrometers. It is believed that the homogeneous *c*-axis orientation in the PEO crystals is controlled by the pathways in developing the maximum crysatllinity within the PEO layers for these PEO-*b*-PS copolymers. One question still remains in this investigation: whether the PEO block tethering density at the interface of the PEO and PS lamellar layers affects the crystal *c*-axis orientation. In this series of copolymers, the tethering densities of the PEO blocks at the interface are 0.33, 0.20, and 0.13 /nm^2 for EOS1, EOS2, and EOS3, respectively. The tethering density decreases with the increased $\bar{M}_n^{PEO}$ and $\bar{M}_n^{PS}$. Does this parameter influence the growth of the PEO crystals with an inclined *c*-axis? One way to investigate this problem may be to blend a low-molecular-weight PEO homopolymer into a diblock copolymer with a PEO cylindrical or sphere phase morphology. Controlling PEO volume fraction by the blending can result in the lamellar phase morphology. Yet within the PEO layers, there are tethered and free PEO chains to tune the tethering density.

Acknowledgment. This work was supported by NSF (DMR-0203994). The 2D SAXS and WAXD research was carried out at the National Synchrotron Light Source in Brookhaven National Laboratory supported by the Department of Energy. We appreciate that Perkin-Elmer Co. sets up a Pyris Diamond DSC in S.Z.D.C.'s laboratory.

References and Notes

(1) Bates, F. S.; Fredrickson, G. H. *Annu. Rev. Phys. Chem.* **1990**, *41*, 525.
(2) Cohen, R. E.; Cheng, P. L.; Douzinas, K. C.; Kofinas, P.; Berney, C. V. *Macromolecules* **1990**, *23*, 324.
(3) Douzinas, K. C.; Cohen, R. E. *Macromolecules* **1992**, *25*, 5030.
(4) Sakurai, K.; MacKnight, W. J.; Lohse, D. J.; Schulz, D. N.; Sissano, J. A. *Macromolecules* **1993**, *26*, 3236.
(5) Cohen, R. E.; Bellare, A.; Drzewinski, M. A. *Macromolecules* **1994**, *27*, 2321.
(6) Khandpur, A. K.; Macosko, C. W.; Bates, F. S. *J. Polym. Sci., Polym. Phys. Ed.* **1995**, *33*, 247.
(7) Hamley, I. W.; Fairclough, J. P. A.; Ryan, A. J.; Bates, F. S.; Towns-Andrews, E. *Polymer* **1996**, *37*, 4425.
(8) Zhao, J.; Majumdar, B.; Schulz, M. F.; Bates, F. S.; Almdal, K.; Mortensen, K.; Hajduk, D. A.; Gruner, S. M. *Macromolecules* **1996**, *29*, 1204.
(9) Liu, L. Z.; Yeh, F.; Chu, B. *Macromolecules* **1996**, *29*, 5336.
(10) Hamley, I. W.; Fairclough, J. P. A.; Terrill, N. J.; Ryan, A. J.; Lipic, P. M.; Bates, F. S.; Towns-Andrews, E. *Macromolecules* **1996**, *29*, 8835.
(11) Zhu, L.; Chen, Y.; Zhang, A.; Calhoun, B. H.; Chun, M.; Quirk, R. P.; Cheng, S. Z. D.; Thomas, E. L.; Hsiao, B. S.; Yeh, F.; Hashimoto, T. *Phys. Rev. B* **1999**, *60*, 10022.
(12) Weimann, P. A.; Hajduk, D. A.; Chu, C.; Chaffin, K. A.; Brodil, J. C.; Bates, F. S. *J. Polym. Sci., Polym. Phys. Ed.* **1999**, *37*, 2053.
(13) Zhu, L.; Cheng, S. Z. D.; Calhoun, B. H.; Ge, Q.; Quirk, R. P.; Thomas, E. L.; Hsiao, B. S.; Yeh, F.; Lotz, B. *J. Am. Chem. Soc.* **2000**, *122*, 5957.
(14) Zhu, L.; Calhoun, B. H.; Chun, M.; Quirk, R. P.; Cheng, S. Z. D.; Thomas, E. L.; Lotz, B.; Hsiao, B. S.; Yeh, F.; Liu, L. *Macromolecules* **2001**, *34*, 1244.
(15) Zhu, L.; Cheng, S. Z. D.; Calhoun, B. H.; Ge, Q.; Quirk, R. P.; Thomas, E. L.; Hsiao, B. S.; Yeh, F.; Lotz, B. *Polymer* **2001**, *42*, 5829.
(16) Zhu, L.; Brion, R. M.; Ge, Q.; Quirk, R. P.; Cheng, S. Z. D.; Thomas, E. L.; Lotz, B.; Hsiao, B. S.; Yeh, F.; Liu, L. *Polymer* **2001**, *42*, 9121.
(17) Loo, Y. L.; Register, R. A.; Ryan, A. J.; Dee, G. T. *Macromolecules* **2001**, *34*, 8968.
(18) Loo, Y. L.; Register, R. A.; Ryan, A. J. *Macromolecules* **2002**, *35*, 2365.
(19) Quiram, D. J.; Register, R. A.; Marchand, G. R. *Macromolecules* **1997**, *30*, 4551.
(20) Quiram, D. J.; Register, R. A.; Marchand, G. R.; Ryan, A. J. *Macromolecules* **1997**, *30*, 8338.
(21) Quiram, D. J.; Register, R. A.; Marchand, G. R.; Adamson, D. H. *Macromolecules* **1998**, *31*, 4891.
(22) Xu, J.-T.; Fairclough, J. P. A.; Mai, S.-M.; Ryan, A. J.; Chaibundit, C. *Macromolecules* **2002**, *35*, 6937.
(23) Xu, J.-T.; Fairclough, J. P. A.; Mai, S.-M.; Chaibundit, C.; Mingvanish, M.; Booth, C.; Ryan, A. J. *Polymer* **2003**, *44*, 6843.
(24) Xu, J.-T.; Turner, S. C.; Fairclough, J. P. A.; Mai, S.-M.; Ryan, A. J.; Chaibundit, C.; Booth, C. *Macromolecules* **2002**, *35*, 3614.
(25) Chaibundit, C.; Mingvanish, W.; Booth, C.; Mai, S.-M.; Turner, S. C.; Fairclough, J. P. A.; Ryan, A. J.; Pissis, P. *Macromolecules* **2002**, *35*, 4838.
(26) Mortensen, K.; Brown, W.; Almdal, K.; Alami, E.; Jada, A. *Langmuir* **1997**, *13*, 3635.
(27) Viras, K.; Kelarakis, A.; Havredaki, V.; Mai, S.-M.; Ryan, A. J.; Mistry, D.; Mingvanish, W.; MacKenzie, P.; Booth, C. *J. Phys. Chem. B* **2003**, *107*, 6946.
(28) Quirk, R. P.; Kim, J.; Kausch, C.; Chun, M. S. *Polym. Int.* **1996**, *39*, 3.
(29) Alexander, L. E. *X-ray Diffraction Methods in Polymer Science*; Wiley-Interscience: New York, 1969.
(30) Cheng, S. Z. D.; Wunderlich, B. *J. Polym. Sci., Polym. Phys. Ed.* **1986**, *24*, 577.
(31) Matsen, M. W.; Bates, F. S. *Macromolecules* **1996**, *29*, 1091.
(32) Shull, K. R. *Macromolecules* **1992**, *25*, 2122.
(33) Takahashi, Y.; Tadokoro, H. *Macromolecules* **1973**, *6*, 672.
(34) Song, K.; Krimm, S. *Macromolecules* **1989**, *22*, 1504.
(35) Song, K.; Krimm, S. *Macromolecules* **1990**, *23*, 1946.
(36) Kim, I.; Krimm. S. *Macromolecules* **1996**, *29*, 7186.
(37) Wunderlich, B. *Macromolecular Physics, Crystal Structure, Morphology, Defects*; Academic Press: New York, 1973; Vol. 1.
(38) Keller, A.; Cheng, S. Z. D. *Polymer* **1998**, *39*, 4461.
(39) Cheng, S. Z. D.; Keller, A. *Annu. Rev. Mater. Sci.* **1998**, *28*, 553.
(40) Reiter, G.; Sommer, J.-U. *J. Chem. Phys.* **2000**, *112*, 4376.
(41) Reiter, G.; Castelein, G.; Sommer, J.-U. *Phys. Rev. Lett.* **2001**, *86*, 5918.
(42) Chen, E.; Jing, A. J.; Weng, X.; Huang, P.; Lee, S.-W.; Cheng, S. Z. D.; Hsiao, B. S.; Yeh, F. *Polymer* **2003**, *44*, 6051.

MA0305378